Journal of Alloys and Compounds, 190 (1992) 17–24
JALCOM 406

Surface and bulk properties of $LaNi_{5-x}Si_x$ alloys from the viewpoint of battery applications

F. Meli, A. Zuettel and L. Schlapbach
Institut de Physique, Université de Fribourg, CH-1700 Fribourg (Switzerland)

(Received May 11, 1992)

Abstract

Because of their rather low hydrogen storage capacity, $LaNi_{5-x}Si_x$ alloys have not been studied well up to now and not considered for battery applications. We have found, however, that the alloy $LaNi_{4.5}Si_{0.5}$ shows fast activation and an incredibly high stability upon electrochemical cycling (-0.07 m A h g^{-1} $cycle^{-1}$) with a fairly high electrochemical capacity (245 m A h g^{-1}). X-ray diffraction, pressure–composition isotherms and electrochemical measurements have been carried out on $LaNi_{4.7}Si_{0.3}$ and $LaNi_{4.5}Si_{0.5}$. By means of photoelectron spectroscopy we have analysed the composition and thickness of surface layers formed on $LaNi_{4.5}Si_{0.5}$ powder electrodes after various pretreatments. Electrochemical cycling in 6 M KOH electrolyte forms a sublayer rich in metallic nickel. Contrary to earlier suggestions, no passivating silicon surface oxide film could be found on cycled $LaNi_{4.5}Si_{0.5}$ electrodes. We attribute the fast activation of these alloys to the very thin oxide layer and to metallic nickel just under the surface, and we attribute the high corrosion resistance to the low volume expansion upon hydriding and the compact surface layer which is therefore formed.

1. Introduction

The process of replacing the toxic cadmium electrodes in rechargeable Ni/Cd batteries by AB_5-type metal hydride electrodes with higher capacity is in full progress [1–4]. The change in the last few years from $LaNi_5$ to $LaNi_5$-based multicomponent alloys has led to an important improvement in battery electrode properties. Many different electrode alloy compositions have been proposed and tested [1–9]. In particular, Willems [6] managed to increase the corrosion stability by replacing nickel partly by cobalt and small amounts of aluminium or silicon. Willems found a higher cycle life the more nickel he substituted by cobalt, and he attributed this to the smaller volume expansion on hydride formation. The further significant improvement in the cycle life due to the addition of small amounts of aluminium or silicon was attributed by Willems and others [2, 5–9] to the formation of a passivating oxide film on the surface. Up to now cobalt was thought to be indispensable for a stable AB_5-type electrode [2, 6].

Earlier we found that the cycle life of $LaNi_{4.7}Al_{0.3}$ was comparable with that of $LaNi_{2.5}Co_{2.5}$ [10] and that no passivating aluminium surface oxide layer was formed on electrochemically cycled $LaNi_{4.7}Al_{0.3}$ electrodes. The improved cycle life was suggested to be caused by the bulk mechanical properties and a higher resistance to disproportionation.

Silicon substitutions lower the plateau pressure, although the lattice constants of $LaNi_{4.5}Si_{0.5}$ do not change with respect to $LaNi_5$. The volume change on hydride formation of $LaNi_{4.5}Si_{0.5}$ is even smaller than for $LaNi_{2.5}Co_{2.5}$, but the hydrogen storage capacity also decreases with increasing silicon content [6, 8, 11–13]. Osumi *et al.* [14] investigated the hydrogen gas absorption of $Mm(Ni, Si)_5$ alloys (Mm = misch metal) and found easy activation, good kinetics, a lower equilibrium pressure and a smaller capacity compared to $MmNi_5$.

Therefore it would be interesting to measure the influence of silicon on the electrochemical cycle life and surface properties of AB_5 electrodes. The surface properties are not only crucial in relation to corrosion but also affect the electrical conductivity, self-discharge and hydrogen–oxygen recombination which have to occur during overcharging in closed cells [15, 16].

We report on X-ray diffraction, pressure–composition isotherms and electrochemical stability measurements of $LaNi_{4.7}Si_{0.3}$ and $LaNi_{4.5}Si_{0.5}$ and on surface analysis of $LaNi_{4.5}Si_{0.5}$ using X-ray photoelectron spectroscopy (XPS).

2. Experimental details

Lanthanum (99.9%) was obtained from Research Chemicals, AZ, USA, nickel (99.99%) from John-

0925-8388/92/$5.00

son–Matthey, UK and silicon (99.999%) from Lonza, Switzerland. The $LaNi_{4.7}Si_{0.3}$ and $LaNi_{4.5}Si_{0.5}$ intermetallic compounds were prepared by r.f. levitation melting of the appropriate amounts of elements in a cooled copper crucible under 10 mbar argon atmosphere and annealed under vacuum ($p < 10^{-6}$ mbar) at 900 °C for 5 days. $LaNi_5$ (Hystor 205) and $LaNi_{4.7}Al_{0.3}$ (Hystor 207) were obtained from Ergenics [17]. The crushed lumps were activated and pulverized through two temperature and pressure hydrogen cycles. This sample pretreatment is called "as received" in what follows.

Powder X-ray diffraction analyses (Debye–Scherrer) were made to determine the structure and lattice parameters of the alloys and their hydrides. The alloys were ground under argon and then put under hydrogen gas pressure up to 30 bar directly into glass capillary tubes of 0.5 mm diameter and 0.01 mm wall thickness (Mark tubes made of Lindemann glass obtained from Hilgenberg, Germany). After cooling to liquid nitrogen temperature the hydrogen was pumped away and the capillaries were sealed. The glass capillaries could safely withstand 30 bar; however, since the volume dilatation of the alloy sometimes caused them to crack, the glass capillary of 0.5 mm diameter with the alloy inside was put into another one of 0.8 mm diameter.

Pressure–composition isotherms were measured dynamically (quasi-equilibrium or continuous method) with alloy samples of mass 2 g. At a constant hydrogen flow rate of 1 $scm^3\ min^{-1}$ (g alloy)$^{-1}$ (scm^3, standard cubic centimetres; $T = 20$ °C; $p = 1013.3$ mbar; Brooks gas flow controller) the pressure was continuously recorded by means of a piezoresistive pressure transducer and a computer. The total error for pressure, flow and mass was smaller than 1% and the temperature of the pressure vessel (total volume 8 cm^3) was controlled with a water bath to ± 0.1 °C. The curves shown consist of about 350 measured points and were corrected for the empty volume in the vessel.

For the electrochemical cycle life measurements approximately 25 mg of active material were mixed with copper powder (Merck p.a.) in a mass ratio of 1:3 and were then cold pressed to a pellet ($d = 7$ mm, $p = 5 \times 10^8$ Pa). To obtain copper-free pellets which could be surface analysed by XPS, the active material (about 80 mg) was pressed into a high void nickel foam and clamped between two fine nickel meshes. All the samples in contact with KOH were extensively rinsed with doubly distilled water, dried in air and subsequently introduced into the ultrahigh vacuum of the photoelectron spectrometer. The electrodes were electrochemically charge–discharge cycled using a computer-controlled current source in 6 M KOH electrolyte. The charge current was 200–400 mA g^{-1} and the discharge current 160 mA g^{-1} (one charge–discharge cycle in about 3 h; the end of the discharge was set to -0.6 V with respect to an Hg/HgO/6 M KOH reference electrode. A platinum foil in a separate compartment was used as a counterelectrode. The cell always contained about 90 ml KOH and was not purged with N_2.

The relative concentrations of the elements and their chemical states at the surface were analysed by XPS in a VG Escalab 5 spectrometer using Mg Kα radiation of energy 1253.6 eV (Au $4f_{7/2}$ at 84.0 eV; full width at half-maximum, FWHM = 1.8 eV). The probe depth is approximately 10–20 Å and the measured surface composition is an average over an area of 0.2 cm^2. To measure depth profiles, Ar^+ ion bombardment (sputtering) at 2 kV was used. The approximate sputter depths indicated were calculated with a standard rate of 500 Å $cm^2\ min^{-1}\ mA^{-1}$ (effectively 4 Å min^{-1}) and are therefore only accurate to a factor of 2 (about 10% relative error between two depth profiles). Since fine powders were analysed, the surface layer changes averaged over the analysed surface are not as sharp as they would be on a plane surface. The phenomenon of "preferential sputtering" also has to be taken into account. It could result in the reduction of metal oxides (especially for the less stable ones) or possibly in the formation of oxides from hydroxides. However, our own experiments on nickel oxide and oxidized $LaNi_5$ showed that only after prolonged sputtering (corresponding to an approximate sputter depth of about 120 Å) did some metallic nickel appear.

3. Results

3.1. X-ray diffraction

The two compounds were single phase and of hexagonal structure. The lattice constants are summarized in Table 1. The dehydrided alloys have almost the same lattice constants as $LaNi_5$, although the Si atoms are smaller than the N atoms [11, 12, 18]. The volume expansion on hydriding, $\Delta V/V$, decreases almost linearly with increasing silicon content, the decrease being almost proportional to the decrease in hydrogen content of the hydrides. For $LaNi_{4.5}Si_{0.5}$ the lattice expansion was only along the a axis, while $LaNi_{4.7}Si_{0.3}$ also showed a small expansion of the c axis. The $LaNi_{5-x}Co_x$ system behaves similarly with $x = 2.3$ and 3.3 respectively [6, 8]. Lartigue and coworkers [11, 12] also measured by neutron diffraction for $LaNi_{4.5}Si_{0.5}D_{4.3}$ a small expansion along the c axis ($a = 5.328(1)$ Å, $c = 4.077(1)$ Å), which could be due to more dissolved deuterium in the β phase at this higher deuterium content.

3.2. Pressure–composition isotherms

Figure 1 shows the dynamically measured pressure–composition isotherm curves for absorption and

TABLE 1. Lattice parameters and volume expansion on hydriding, $\Delta V/V$, for silicon-substituted $LaNi_5$-based alloys compared with $LaNi_5$ [6]

Alloy	H:M approx.	Hydrided		Dehydrided		$\Delta a/a$ (%)	$\Delta c/c$ (%)	$\Delta V/V$ (%)
		a (Å)	c (Å)	a (Å)	c (Å)			
$LaNi_5$	6	5.395	4.244	4.999	3.988	7.9	6.4	23.9
$LaNi_{4.7}Si_{0.3}$	4.4	5.322(7)	4.118(6)	4.992(3)	3.979(3)	6.6	3.5	17.6(7)
$LaNi_{4.5}Si_{0.5}$	3.5	5.285(7)	3.990(8)	4.992(4)	3.978(8)	5.9	0.3	12.4(9)

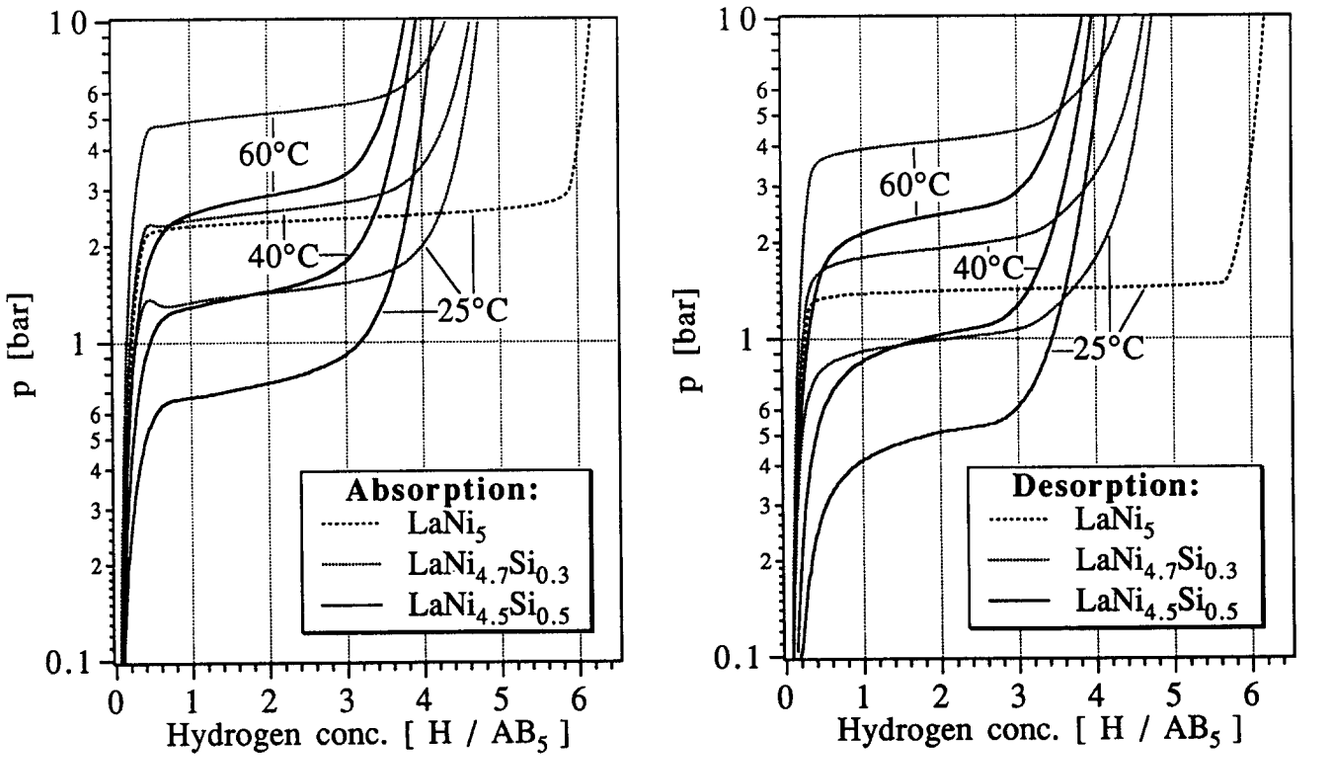

Fig. 1. Dynamic absorption–desorption pressure–composition isotherms for the La(Ni, Si)$_5$–H system at a constant hydrogen flow rate of 1 scm^3 min^{-1} (g alloy)$^{-1}$.

desorption. The curve for $LaNi_5$, which is included for comparison, shows a very flat desorption plateau with a slope of only 0.07 bar/H:AB$_5$ = 1–5) and very sharp transitions from the α phase to the $\alpha+\beta$ region and from the $\alpha+\beta$ region to the β phase at 0.35 and 5.65 H:$LaNi_5$ respectively. Interestingly, the plateau slope is higher for absorption, 0.3 bar/(H:AB$_5$ = 1–5), as already observed earlier [19]. Relative to $LaNi_5$ the silicon-substituted alloys show lower plateau pressures, shorter plateaux and a little higher plateau slopes, although the structure and lattice constants are the same as those of $LaNi_5$. Lartigue found an equilibrium pressure for desorption of 0.44 bar at 25 °C for $LaNi_{4.5}Si_{0.5}$ [11], which is 0.06 bar less than the value we found. The transition from the α phase to the $\alpha+\beta$ region for the $LaNi_{4.7}Si_{0.3}$ compound is almost as abrupt as for $LaNi_5$; at lower temperatures it is smoother, probably owing to slower kinetics. (See also the bumps on the absorption curves for $LaNi_{4.7}Si_{0.3}$.) The α phase of $LaNi_{4.5}Si_{0.5}$ is more extended. For both alloys the β phase begins already at H:AB$_5$ = 2.7. The hydrogen solubility in the β phase is highest for $LaNi_{4.7}Si_{0.3}$, while it is smaller for $LaNi_{4.5}Si_{0.5}$ and $LaNi_5$. Thus silicon causes a strong decrease in the hydrogen gas storage capacity, which corresponds at 25 °C and 3 bar to an electrochemical capacity of 280 mA h g^{-1} for $LaNi_{4.7}Si_{0.3}$ and 245 mA h g^{-1} for $LaNi_{4.5}Si_{0.5}$.

For both compounds the hysteresis $\ln(p_{abs}/p_{des})$ was the same except at 60 °C (Table 2) and smaller than that for $LaNi_5$ (0.53 at 25 °C; static, 0.19 [17]), but higher than that for $LaNi_{4.7}Al_{0.3}$ (0.05 at 25 °C, static measurement [17]). Hysteresis measurements with the

TABLE 2. Hydrogen absorption capacity, equilibrium pressures, hysteresis and thermodynamic data for silicon-substituted $LaNi_5$-based alloys

Alloy	H:M 3 bar, 25 °C	25 °C		40 °C		60 °C	
		p_{abs} (bar)	p_{des} (bar)	p_{abs} (bar)	p_{des} (bar)	p_{abs} (bar)	p_{des} (bar)
$LaNi_{4.7}Si_{0.3}$	4.4	1.42	0.99	2.56	1.92	5.18	4.15
$LaNi_{4.5}Si_{0.5}$	3.9	0.72	0.50	1.34	1.01	2.82	2.41

	Hysteresis $\ln(p_{abs}/p_{des})$			$\lvert\Delta H\rvert$ (kJ (mol H_2)$^{-1}$)		$\lvert\Delta S\rvert$ (J (kmol H_2)$^{-1}$)	
	25 °C	40 °C	60 °C	Des.	Abs.	Des.	Abs.
	0.36	0.29	0.22	33.8(2)	30.7(2)	113.1(8)	105.6(6)
	0.36	0.28	0.16	36.5(3)	31.4(4)	116.6(10)	102.9(12)

dynamic method usually give higher values even if they are made very slowly [20]. Hysteresis is associated with plastic deformation and dislocation generation produced by the volume change on hydriding [19]. However, there seems to be no direct relation between hysteresis and electrochemical stability. For example, $LaNi_5$ and $LaNi_{4.7}Al_{0.3}$ have a lower stability than $LaNi_{4.7}Si_{0.3}$.

The enthalpy and entropy changes of absorption and desorption were obtained via least-square fits to the expression

$$\ln\left(\frac{p}{p_0}\right) = \frac{\Delta H}{RT} - \frac{\Delta S}{R} \qquad \text{with } p_0 = 1013 \text{ mbar}$$

For both alloys good fits were obtained and the results are given in Table 2 and in the Van't Hoff plots of Fig. 2. The enthalpy change of desorption for the $LaNi_{4.5}Si_{0.5}$ alloy agrees quite well with the value found by Lartigue [11] (37.3 kJ (mol H_2)$^{-1}$) and with the value for $LaNi_{4.6}Si_{0.4}$ found by Mendelsohn and Gruen [13] (35.6 kJ (mol H_2)$^{-1}$). For both alloys the enthalpy change of desorption was higher than that of absorption, which can be seen by the different slopes of the Van't Hoff plots (Fig. 2).

3.3. Electrochemical cycling

The $La(Ni, Si)_5$ alloys showed very fast activation even with a charge current of 200 mA g^{-1} and a discharge current of 160 mA g^{-1}. Already at the second cycle the capacity was 270 mA h g^{-1} (96%) for $LaNi_{4.7}Si_{0.3}$ and 240 mA h g^{-1} (98%) for $LaNi_{4.5}Si_{0.5}$ (Fig. 3). At cycle number 60 the charge current was doubled to 400 mA g^{-1} (1 h charge); this caused a slight decrease in capacity owing to the lower charge efficiency. The mean discharge potential (the potential averaged over the whole discharge capacity) was still decreasing during the first 20 cycles (to −875 mV *vs.* Hg/HgO/6 M KOH at 160 mA g^{-1} discharge current)

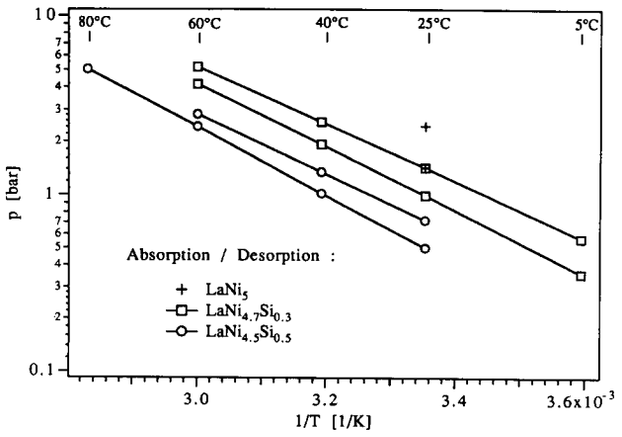

Fig. 2. Van't Hoff plots for absorption and desorption for the $La(Ni, Si)_5$–H system.

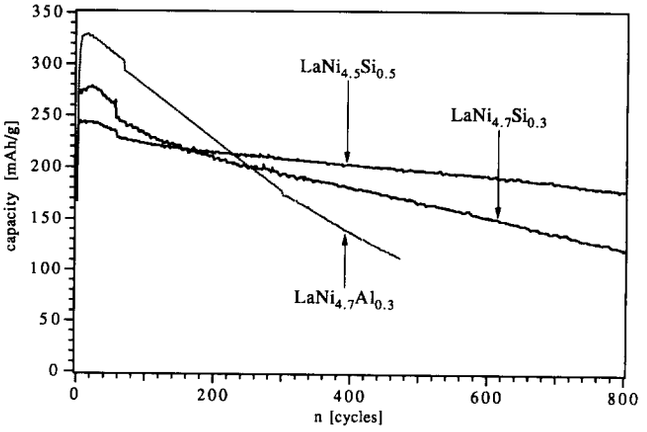

Fig. 3. Discharge capacity *vs.* cycle number of silicon- and aluminium-substituted $LaNi_5$-based electrodes (up to cycle 60, 200 mA g^{-1} and thereafter 400 mA g^{-1} charge current; discharge current 160 mA g^{-1}).

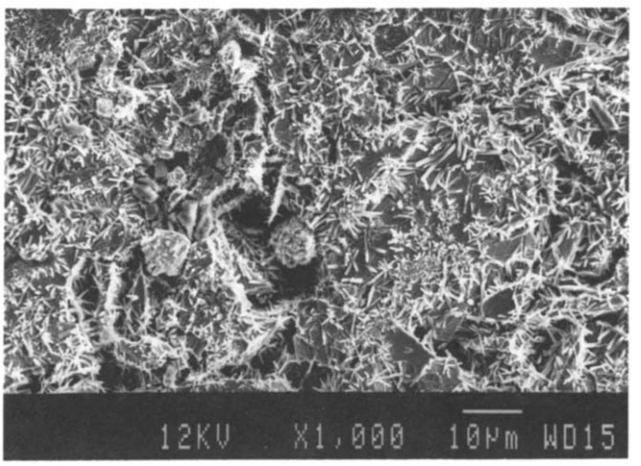

Fig. 4. Scanning electron micrograph of an $LaNi_{4.5}Si_{0.5}$ alloy pressed powder sample which was heated in 6 M KOH to about 100 °C for 1 h, showing $La(OH)_3$ needles (EDXA).

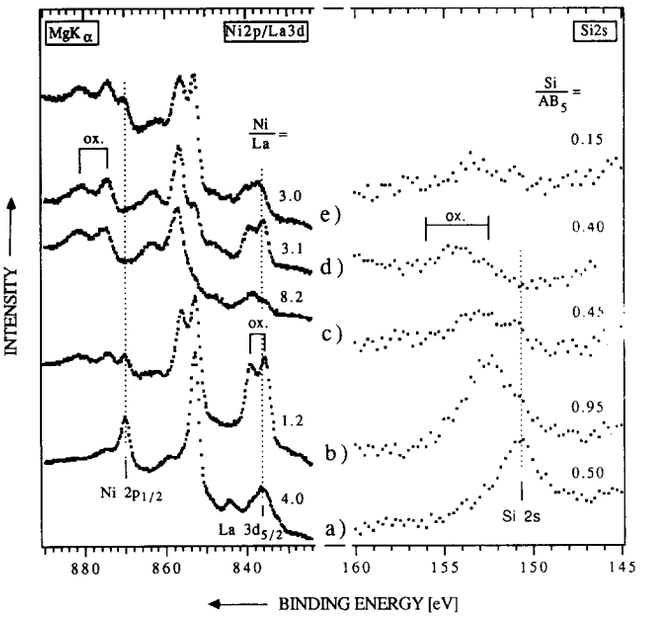

Fig. 5. Ni 2p, La 3d and Si 2s core level spectra of $LaNi_{4.5}Si_{0.5}$ powder electrodes after different pretreatments: (a) prolonged Ar^+ bombardment (sputtered); (b) two hydrogen gas activation cycles ("as received"); (c) stored in 6 M KOH at 22 °C for 24 h at 0 V *vs.* Hg/HgO/6 M KOH reference electrode; (d) heated in 6 M KOH for 1 h to about 100 °C; (e) 30 electrochemical charge–discharge cycles in 6 M KOH; (b)–(e) with transfer in air.

and the open potential after discharge, which indicates to what extent the alloys could be dehydrided, increased up to cycle number 60. In comparison with other stable AB_5 multicomponent electrodes this is a very fast activation [6, 21]. The capacity decrease for the $LaNi_{4.5}Si_{0.5}$ compound of only 0.07 mA h g^{-1} $cycle^{-1}$ or 2.8% of initial capacity per 100 cycles was extremely small.

Scanning electron micrographs showed the same grain size distributions and grain surface morphologies for samples after two hydrogen cycles and for samples after 30 electrochemical cycles, *i.e.* the micrographs could not be distinguished. Scanning electron microscopy (SEM) and energy-dispersive X-ray analysis (EDXA) of $LaNi_{4.5}Si_{0.5}$ alloy samples which were heated in 6 M KOH to about 100 °C for 1 h showed that the grains were covered with $La(OH)_3$ needles (Fig. 4). Probably because of the low solubility of $La(OH)_3$ in 6 M KOH [3, 22], it precipitates back to the surface in the form of needles. Surprisingly, the so-treated $LaNi_{4.5}Si_{0.5}$ alloy still had its full capacity of 245 mA h g^{-1} at 160 mA g^{-1} discharge current! Thus no active lanthanum seems to have been lost.

3.4. *Surface analysis*

Figure 5 shows the La 3d and Ni 2p core level spectra taken on differently prepared $LaNi_{4.5}Si_{0.5}$ electrode surfaces. Since the La $3d_{3/2}$ and Ni $2p_{3/2}$ peaks overlap (peaks in the middle of the spectra), the La $3d_{5/2}$ and Ni $2p_{1/2}$ peaks were used for evaluation. Because of the small photo-ionization cross-section of the Si 2s core level (the Si 2p peak overlaps with the La 4d peak), a higher uncertainty for the silicon content has to be considered, *i.e.* ±1.5% relative to the total metal content (bulk concentration 8.3%).

(a) After prolonged Ar^+ sputtering we found a ratio Ni:La = 4, the remaining oxygen contamination being about 5%. After Ar^+ sputtering we always found the Ni:La ratio to be slightly lower than the bulk ratio (Ni:La = 4.5). This could be due to the residual oxygen contamination, fast lanthanum surface segregation even during the absence of oxygen [23], weak preferential sputtering or possibly the way in which the XP spectra were evaluated (determination of the peak areas). The surface composition after sputtering corresponds to $La_{1.1}Ni_{4.4}Si_{0.5}$.

(b) The "as-received" $LaNi_{4.5}Si_{0.5}$ sample, *i.e.* after two hydrogen pressure cycles (activation, pulverization) and sample transfer in air, showed an oxygen content at the surface of about 43% and about 20% carbon (adsorbed). Accordingly, the oxygen-induced lanthanum segregation to the surface was strong; the Ni:La ratio amounted to 1.2 and the Si:La ratio to 0.4. This means that silicon was slightly enriched, but not as much as lanthanum. The lanthanum was fully oxidized, but half the nickel was found to be in the metallic state. Upon sputtering, pure metallic nickel was already found after about 4 Å, while lanthanum remained as oxide down to about 80 Å (oxygen penetration depth). Thus there were only about 1 or 2 monolayers of nickel oxide, which is a very thin layer compared to what we found earlier on $LaNi_5$ and $LaNi_{4.7}Al_{0.3}$ [10]. The Si:La ratio

remained approximately constant during sputtering and the Si 2s peak indicated SiO_x down to about 40 Å.

(c) The contact of "as-received" $LaNi_{4.5}Si_{0.5}$ (copper-free pressed powder pellet) with 6 M KOH at 22 °C for 24 h at a slightly oxidizing potential (0 V *vs.* Hg/HgO) induced a strong nickel oxide enrichment at the surface. The Ni:La ratio rose to 8.2 and the Si:La ratio was 0.7. Nickel, silicon and lanthanum were oxidized. Sputtering revealed that the nickel oxide layer was about 15 Å thick. Underneath this, metallic nickel was present in a lanthanum-oxide-rich layer. Silicon was found as SiO_x down to about 40 Å. Apart from the topmost layer for Si:La and below 70 Å for Ni:La only small deviations from the bulk ratios were found (Fig. 6). In agreement with our earlier measurements on $LaNi_5$ and $LaNi_{4.7}Al_{0.3}$ [10], we found a nickel-rich top surface layer, apparently as a result of the dissolution of lanthanum in the electrolyte. The Si:Ni ratio corresponds to the bulk composition also in the top surface layer.

(d) "As-received" alloy samples which were heated in 6 M KOH to about 100 °C for 1 h showed a surface with oxidized nickel, silicon and lanthanum in almost bulk ratios. SEM and EDXA showed that the grains were covered with $La(OH)_3$ needles (Fig. 4). Because of the inhomogeneous surface, XPS depth profiles are difficult to evaluate.

(e) After 30 electrochemical cycles (duration 5 days) the oxygen penetration depth increased to about 400 Å; however, no capacity decrease (within 2%) was found. The composition of the surface layer was generally closer to the bulk value than for the other pretreatments. The Ni:La ratio on the surface was 3.0, increased to 6.0 at a depth of about 40 Å and decreased again to 3.6 at 200 Å. The nickel oxide film on the surface was very thin. Upon sputtering, pure metallic nickel was found already after about 4 Å. Therefore there is a layer from 10 to 100 Å which is rich in metallic nickel (Fig. 6). There was very little silicon at the surface (Si:La = 0.12, Si:Ni = 0.04) and its concentration was even smaller between 10 and 100 Å. Silicon was present as SiO_x down to 100 Å. Down to 30 Å lanthanum was present as hydroxide and down to 400 Å as oxide.

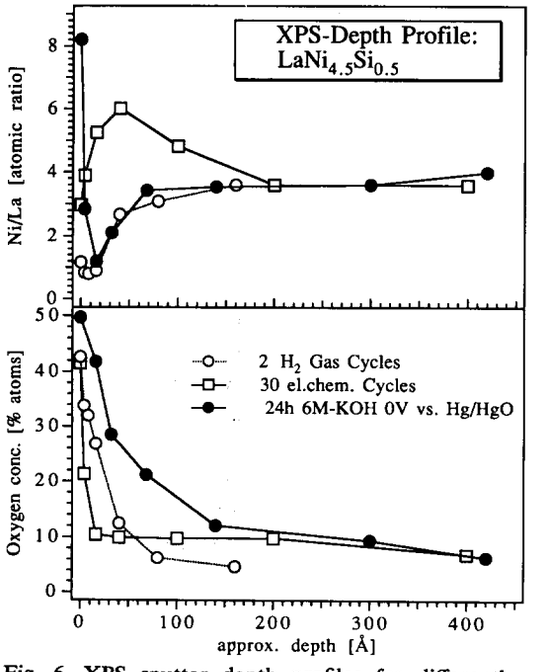

Fig. 6. XPS sputter depth profiles for differently pretreated $LaNi_{4.5}Si_{0.5}$ samples.

4. Discussion

It is apparent that $LaNi_{5-x}Si_x$ intermetallic compounds exhibit very interesting properties from the viewpoint of their use as electrodes in rechargeable batteries. We will now discuss the analysed properties (structure and morphology, electrochemical and surface properties) in order to understand what makes this system better than pure $LaNi_5$.

The $LaNi_{5-x}Si_x$ system has the same structure and almost the same lattice constants as $LaNi_5$, but its properties are quite different. Silicon replaces nickel only in 3*g* positions and deuterium was found on 6*m*, 12*n* and 4*n* sites, while in aluminium- and manganese-substituted compounds deuterium was also found on the 12*o* site [11, 12, 18]. The $LaNi_{5-x}Co_x$ system ($x = 2.3$ resp. 3.3) [6, 8] shows almost the same dilatation of the lattice constants, $\Delta a/a$ and $\Delta c/c$, upon hydriding as the $LaNi_{5-x}Si_x$ system ($x = 0.3$ resp. 0.5); thus the silicon substitutions are more efficient at decreasing the lattice expansion. The low volume dilatation on hydride formation causes a stable grain morphology during electrochemical cycling, and it was possible to sinter the alloy powder with a fine nickel foam, without any binding material, to stable electrodes which did not fall apart during the first 20 electrochemical cycles. Low $\Delta V/V$ also facilitates the production of compact closed cells.

The capacity for hydrogen gas absorption is quite low but, the electrochemical capacity is reasonable for a stable AB_5 alloy, so that together with the high stability on electrochemical cycling, good average capacities can be obtained. (Since the capacity decrease occurs only during cycling and is proportional to the total amount the exchanged hydrogen [24] and because in a battery the capacity would be limited by the positive nickel hydroxide electrode, one can use the average capacity of 200 mA h g^{-1} up to cycle 800 for the design of a battery with the $LaNi_{4.5}Si_{0.5}$ alloy). The plateau pressure, which remains below 1 bar up to 40 °C for $LaNi_{4.5}Si_{0.5}$, is suitable for closed-cell application.

Surface analysis yields drastically different surface compositions depending on the pretreatment. The Ni:La ratios vary from about 1.2 to 8.2. Through electrochemical cycling, a nickel-rich subsurface layer is formed. The concentration of nickel in this layer is higher than that found for $LaNi_{4.7}Al_{0.3}$, while for $LaNi_5$ there was no nickel enrichment [10]. Thus these differences seem to be of relevance for cyclic stability and they could possibly also affect the electrical conductivity, self-discharge and hydrogen–oxygen recombination which have to occur during overcharging.

The nickel oxide layer on the surface of $LaNi_{4.5}Si_{0.5}$ was generally thinner than on $LaNi_{4.7}Al_{0.3}$ [10]. The difference is very pronounced on the "as-received" and cycled electrodes, where we found even in the unsputtered state metallic nickel on the surface, *i.e.* in the information depth of XPS. After only 1 minute of Ar^+ bombardment all the nickel was metallic, so we conclude that there are only 1 or 2 monolayers of nickel oxide, remembering that the samples were transferred through air into the ultrahigh vacuum of the spectrometer. On all the samples we found metallic nickel in a layer underneath the top surface. Interestingly, on the electrochemically cycled electrodes we found a high concentration of metallic nickel, and this layer was thicker and the nickel oxide layer was thinner than on the samples with the other pretreatments. (At the end of each electrochemical cycle the potential of the electrode rises, so that nickel will be oxidized and, during the charging that follows, reduced again:

$$Ni + 2OH^- \longrightarrow Ni(OH)_2 + 2e^-$$

at -816 mV *vs.* Hg/HgO [25]

However, the nickel oxide is passivating and the reaction stops after a few monolayers of $Ni(OH)_2$ have formed. The samples were transferred in the charged state into the XP spectrometer).

It is very often assumed that silicon is much more stable in strong basic solutions than lanthanum. Accordingly, models of passivating silicon oxide layers were proposed to explain the enhanced corrosion stability of silicon-substituted AB_5 compounds. The results of surface analysis contradict this model of a passivating silicon oxide surface layer [2, 6, 8]. A compact silicon or silicon oxide surface layer of only 1 monolayer thickness should indicate with XPS a silicon content greater than 20% (relative to metals). The highest silicon content at the surface (16% relative to metals) was found in the "as-received" sample, while all the others (especially the one after 30 electrochemical cycles) clearly showed less silicon at the surface. At the most, one could possibly think of a surface with nickel islands which is only covered in between with passivating silicon-containing oxides [26].

Furthermore, silicon dissolves faster than lanthanum in strong basic solutions. Elemental silicon and aluminium dissolve readily in 6 M KOH with hydrogen evolution because the corresponding surface oxide layers are not passivating, while nickel and lanthanum do not dissolve because passivating oxide layers are formed. The solubility of $La(OH)_3$ seems to be very low in basic solutions [3, 22]. Lanthanum reacts very strongly with oxygen and hydrogen; therefore the hydrogen-gas-cycled and air-exposed $LaNi_{5-x}Si_x$ compounds show a high lanthanum oxide enrichment at the surface. In 6 M KOH, silicon, silicon oxides and also small amounts of lanthanum oxides are dissolved from the surface, and at a slightly oxidizing potential the nickel oxide gets stronger and thicker so that a passivating film is formed which remains even after rinsing in water and drying in air. This film can inhibit further lanthanum segregation. At potentials below -816 mV, *i.e.* during charging, most of the oxidized nickel is reduced. Because of the continued expansion and shrinkage of the grains upon recycling, new surfaces are created during about the first 60 cycles. Owing to the enhanced mobility of the atoms during phase changes, more silicon and lanthanum segregate to the surface and dissolve. A stable metallic nickel layer is left. Since the volume expansion of these alloys is not high enough to destroy this nickel-rich layer, they have very good corrosion stability on electrochemical cycling. In our opinion it is also this nickel-rich layer that causes somewhat higher overpotentials.

5. Conclusions

The $LaNi_{5-x}Si_x$ system has many interesting properties for its application in battery electrodes, *e.g.* high stability, fast activation, low volume expansion on hydride formation, sinterable and suitable plateau pressure. Silicon substitutes are cheaper and more effective for obtaining certain properties than cobalt substitutes. The $LaNi_{5-x}Si_x$ system could therefore serve as a basis for the development of low cost, multicomponent alloys in combination with Mm, lanthanum rich Mm, aluminium and manganese but without or with very little cobalt.

The surface analysis revealed drastic modifications of the composition and thickness of surface layers formed upon contact of the electrodes with KOH and electrochemical cycling. These modifications seem to be of relevance for corrosion.

No passivating silicon surface oxide layer was found on electrochemically cycled $LaNi_{4.5}Si_{0.5}$ electrodes. The improved cycle life is suggested to be caused by the low volume expansion upon hydriding and the compact nickel-rich surface layer which is therefore formed. The

fast activation is probably due to the thin nickel oxide layer formed on these alloys.

Acknowledgment

Financial support by the Swiss Department of Energy (BEW) is acknowledged.

References

1 T. Sakai, H. Yosinaga, H. Miyamura, N. Kuriyama and H. Ishikawa, *J. Alloys Comp., 180* (1992) 37.
2 T. Sakai, T. Hazama, H. Miyamura, N. Kuriyama, A. Kato and H. Ishikawa, *J. Less-Common Met., 172–174* (1991) 1175.
3 M. Kanda, M. Yamamoto, K. Kanno, Y. Satoh, H. Hayashida and M. Suzuki, *J. Less-Common Met., 172–174* (1991) 1227.
4 G. Sandrock, S. Suda, L. Schlapbach, Applications, in L. Schlapbach (ed.), *Topics in Applied Physics,* Vol. 67, *Hydrogen in Intermetallic Compounds II,* Springer, Berlin, 1992, Chap. 5.
5 A. Percheron, J. C. Achard, J. Sarradin and G. Bronoël, *Proc. Int. Symp. on Hydrides for Energy Storage, Geilo, 1977,* p. 485.
6 J. J. G. Willems, *Philips Res. J., 39* (Suppl. 1) (1984) 1.
7 T. Sakai, H. Miyamura, N. Kuriyama, A. Kato, K. Oguro and H. Ishikawa, *J. Electrochem. Soc., 137* (1990) 795.
8 T. Sakai, K. Oguro, H. Miyamura, N. Kuriyama, A. Kato, H. Ishikawa and C. Iwakura, *J. Less-Common Met., 161* (1990) 193.
9 T. Sakai, H. Miyamura, N. Kuriyama, A. Kato, K. Oguro, H. Ishikawa and C. Iwakura, *J. Less-Common Met., 159* (1990) 127.
10 F. Meli and L. Schlapbach, *J. Less-Common Met., 172–174* (1991) 1252.
11 C. Lartigue, *Thesis,* Université Pierre et Marie Curie, Paris 6, 1984.
12 J. C. Achard, A. J. Dianoux, C. Lartigue, A. Percheron-Guégan and F. Tasset, in G. J. McCarthy, J. J. Rhyne and H. B. Silver (eds.), *The Rare Earths in Modern Science and Technology,* Vol. 3, Plenum, New York, 1982, p. 481.
13 H. M. Mendelsohn and D. M. Gruen, in G. J. McCarthy and J. J. Rhyne (eds.), *Rare Earths in Modern Science and Technology,* Plenum, New York, 1980, p. 593.
14 Y. Osumi, H. Suzuki, A. Kato and M. Nakane, *J. Less-Common Met., 84* (1982) 99.
15 C. Iwakura, Y. Kajiya, H. Yoneyama, T. Sakai, K. Oguro and H. Ishikawa, *J. Electrochem. Soc., 136* (1989) 1351.
16 T. Sakai, A. Yuasa, H. Ishikawa, H. Miyamura and N. Kuriyama, *J. Less-Common Met., 172–174* (1991) 1194.
17 E. L. Huston and G. D. Sandrock, *J. Less-Common Met., 74* (1980) 435.
18 A. Percheron-Guégan, C. Lartigue and J. C. Achard, *J. Less-Common Met., 109* (1985) 287.
19 T. B. Flanagan and W. A. Oates, Thermodynamics of intermetallic compounds–hydrogen systems, in L. Schlapbach (ed.), *Topics in Applied Physics,* Vol. 63, *Hydrogen in Intermetallic Compounds I,* Springer, Berlin, 1988, Chap. 3, p. 49.
20 P. D. Goodell, G. D. Sandrock and E. L. Houston, *J. Less-Common Met., 73* (1980) 135.
21 A. H. Boonstra, T. N. M. Bernards and G. J. M. Lippits, *J. Less-Common Met., 159* (1989) 327.
22 D. C. Lewis, *Chem. Ind. (Lond.),* (1957) 1238.
23 L. Schlapbach and C. R. Brundle, *J. Phys. (Paris) 42* (1981) 1025.
24 A. H. Boonstra, G. J. M. Lippits and T. N. Bernards, *J. Less-Common Met., 155* (1989) 119.
25 M. Pourbaix, *Atlas of Electrochemical Equilibria,* NACE, Cebelcor, Brussels, 1974, p. 331.
26 J. J. G. Willems and K. H. J. Buschow, *J. Less-Common Met., 129* (1987) 13.